

CABLE DESIGN FOR FAST RAMPED SUPERCONDUCTING MAGNETS (*Cos- θ* DESIGN)

A.K. Ghosh

Brookhaven National Laboratory, Upton, New York, USA

Abstract

The new heavy ion synchrotron facility proposed by GSI will have two superconducting magnet rings in the same tunnel, with rigidities of 300 T-m and 100 T-m. Fast ramp times are needed, which can cause significant problems for the magnets, particularly in the areas of ac loss and magnetic field distortion. The development of the low loss Rutherford cable that can be used is described, together with a novel insulation scheme designed to promote efficient cooling. Measurements of contact resistance in the cable are presented and the results of these measurements are used to predict the ac losses, in the magnets during fast ramp operation. For the high energy ring, a 1m model dipole magnet was built, based on the RHIC dipole design. This magnet was tested under boiling liquid helium in a vertical cryostat. The quench current showed very little dependence on ramp rate. The ac losses, measured by an electrical method, were fitted to straight line plots of loss/cycle versus ramp rate, thereby separating the eddy current and hysteresis components. These results were compared with calculated values, using parameters which had previously been measured on short samples of cable. Reasonably good agreement between theory and experiment was found, although the measured hysteresis loss is higher than expected in ramps to the highest field levels.

1. INTRODUCTION

GSI is planning a new heavy ion accelerator consisting of two superconducting synchrotron rings placed one above the other in the same tunnel [1], and ramping with a rise time of a few seconds. The lower ring, having a magnetic rigidity of 100 T-m, will use magnets based on the Nuclotron design [2]. The upper ring was originally planned to be 200 T-m and use magnets based on the RHIC design [3], but this ring has recently been increased to 300 T-m. As a prototype for the original 200 T-m ring, a 1m long model dipole was built, based on the RHIC single layer *cos- θ* design, but with various modifications to enable high ramp rates. The model was successfully tested for quench behaviour and ac losses at ramp rates up to 4T/s:

To date, superconducting accelerators with high field magnets have all worked at relatively slow ramp rates and have been able to use Rutherford cable without incurring too much ac loss. At high ramp rates ~ 1 T/s however, coupling between the strands of a conventional Rutherford cable would produce high ac losses and unacceptable field distortion. Coupling may be reduced by increasing the resistance between strands in the cable (by coating the strands with a highly resistive coating), but there are reasons to believe that this can impede current sharing and thereby make the magnet more susceptible to quenching at high ramp rates. Because coupling in Rutherford cables is very anisotropic, it may be reduced greatly by increasing the crossover resistance via a resistive core foil, while still leaving a low resistance in the other direction. Cables with Kapton-core foils were first tried more than 20 years ago [4] and have been the subject of ongoing research. We show that cores reduce the coupling losses without affecting the quench performance of magnets.

In this paper we describe the development of a low loss Rutherford cable suitable for use in fast ramping magnets, using the RHIC strand and cable as the starting point. The losses arising from the strand and cable are examined and a suitable selection of the cable is made which is fabricated and wound into single layer coils. Following that, the quench behavior and the losses of a prototype magnet is described. Most of what is presented here can be found in earlier publications, Ref. [5-9]

The parameters of the RHIC strand and cable are in Table 1, and the wire cross-section is shown in Fig. 1.

Table 1:
Parameters of the RHIC Cable

Wire diameter (mm)	d_w	0.648
Filament diameter (mm)	d_f	6.0
Cu/Sc ratio	m	2.25
Wire twist pitch (mm)	L_w	13
Wire coating		None, (bare copper)
No. of strands in cable	N	30
Cable width (mm)	$2c$	9.73
Cable mid-thickness (mm)	$2b$	1.166
Cable Keystone angle (deg)		1.2
Cable lay pitch (mm)	p	74

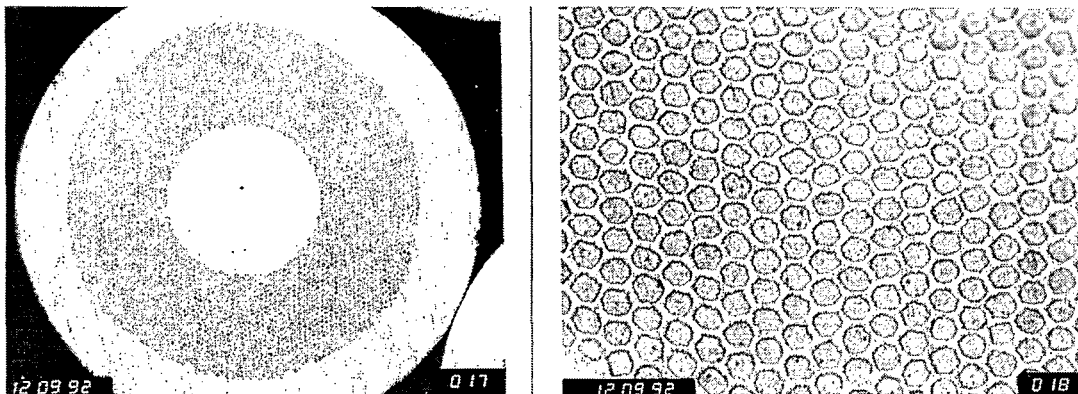


Fig. 1 RHIC strand cross-section

2. CABLE DESIGN

2.1 Strand losses.

At the strand level, the eddy current magnetization (and losses) due to a changing B-field transverse to the wide face of a cable, \dot{B} is controlled by the wire twist pitch and the inter-filament matrix resistivity and is given by

$$M_e = \frac{2\dot{B}\tau_f}{\mu_o} \quad (1)$$

where τ_f is the inter-filament coupling time constant

$$\tau_f = \frac{\mu_0}{2\rho_{et}} \left\{ \frac{L_w}{2\pi} \right\}^2 \quad (2)$$

and ρ_{et} is the effective transverse resistivity across the wire, depending on the copper matrix, the interface resistance between NbTi and copper, and the geometry. In the case of the RHIC strand which has copper as the interfilament matrix, $\rho_{et} \sim 1.0 \times 10^{-10} \Omega \cdot m$. This was calculated from magnetization measurements made at CERN [10] on annealed strand. To reduce this loss component, the twist pitch was reduced from 13mm to 3mm. However for the very tight twist pitch the critical current density, J_c , of the wire degrades as shown in Fig. 2.

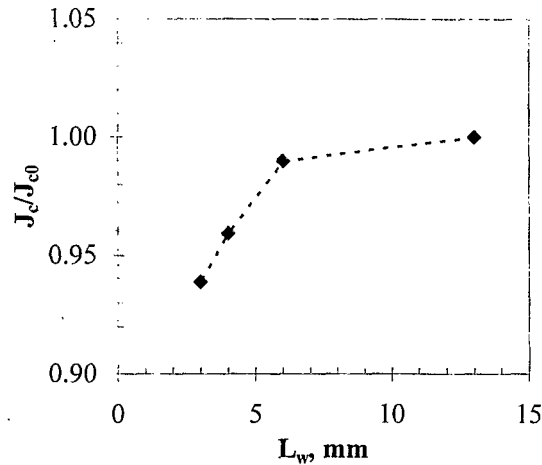


Fig. 2 J_c/J_{c0} as a function of twist pitch for the RHIC strand

Hence for the prototype magnet the strand was chosen with a twist pitch of 4mm, which reduces the filament-coupling by an order of magnitude, without a significant loss of J_c . In the future increasing the matrix resistivity by using Cu-0.5%Mn alloy might be a better option to further reduce this component of eddy-current loss [11].

2.2 Cable Losses

In Rutherford cables, the dominant source of loss in changing transverse field is due to the inter-strand coupling magnetization, that are determined by the strand *crossover resistance* R_c and the strand *adjacent resistance* R_a as shown in Fig 3. (Reproduced from Ref. [6])

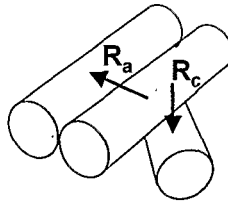


Fig. 3 Crossover and adjacent resistances between strands in a cable (note that R_a is defined to be over the same length of wire that R_c occupies).

The eddy currents flowing between the strands can be suppressed by increasing these inter-strand resistances, however very high R_a and R_c could lead to quench current degradation in magnets at high

ramp rates due to a lack of current sharing between the strands. In the absence of a definite theory, we have therefore decided to make the contact resistance high enough to control the losses, but no higher than necessary. To quantify how high, we need to look at the three types of inter-strand coupling in Rutherford cable.

a) *Cable coupling via R_c in transverse field*

$$M_{tc} = \frac{1}{120} \frac{\dot{B}_t}{R_c} \frac{c}{b} p N(N-1) \quad (4)$$

where M_{tc} is the magnetization per unit volume of cable, p is the cable twist pitch, \dot{B}_t is the rate of change of field transverse to the broad face of the cable, N is the number of strands, c is the half width of the cable and b is its half thickness.

b) *Cable coupling via R_a in transverse field*

$$M_{ta} = \frac{1}{6} \frac{\dot{B}_t}{R_a} p \frac{c}{b} \quad (5)$$

where M_{ta} is the coupling magnetization due to R_a in transverse magnetic field.

c) *Cable coupling via R_a in parallel field*

$$M_{pa} = \frac{1}{8} \frac{\dot{B}_p}{R_a} p \frac{b}{c} \quad (6)$$

where \dot{B}_p is the rate of change of field parallel to the broad face of the cable. Because c is always much greater than b , it may be seen immediately that the loss in transverse field is much greater than in parallel field. From (4) and (5) we see that the ratio is:

$$\frac{M_{tc}}{M_{ta}} = \frac{R_a}{R_c} \left\{ \frac{N}{20} (N-1) \right\} \quad (7)$$

A typical value for the factor in brackets is ~ 50 , which means that a given crossover resistance causes 50 times more loss than the same adjacent resistance. It follows that we can make $R_a \sim R_c / 50$ without increasing the loss too much. It is this inherent anisotropy in the loss mechanism that is the reason for choosing cored cables. For the SIS200 prototype magnet designed to operate to 4T at 1T/s, a target value of $50 \mu\Omega$ for R_a and $5 \text{ m}\Omega$ for R_c was set.

2.2.1 Cored-cable development

The RHIC cable was chosen for this development as strands were readily available and since the prototype magnet was based on the RHIC design. For bare copper strands it is known that the inter-strand resistance is very variable due to the oxide that develops on the surface of the bare wire. R_a and R_c can vary significantly from cable to cable and with the coil-curing heat-pressure cycle that is utilized in coil fabrication. Following LHC where Sn-4%Ag solder coated strands are used to control cable R_c in the magnets, it was decided to coat the RHIC strands with $\sim 1 \mu\text{m}$ of Sn-4%Ag to control R_a . Additionally the wire diameter was reduced to 0.638mm in order to accommodate a 25 mm thick resistive core without over compacting the RHIC cable.

During the development of cored-cables, several different foils have been tried, namely:

- a. 25 μm thick stainless steel 304, annealed
- b. 25 μm thick stainless steel 316, annealed
- c. 25 μm thick anodized titanium
- d. 25 μm thick Cu-30wt%Ni (CDA 715), half-hard and annealed

- e. 50 μm thick Brass
- f. 75 μm thick Kapton

Tapes were all 8mm wide which is the maximum size that can be used without problems at the edges. Fig. 3 and 4 shows a cross-section of the cored cable.

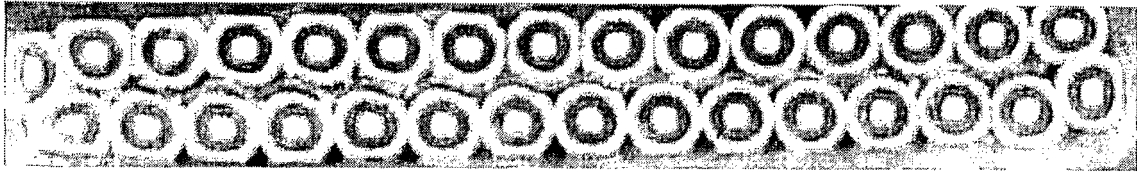


Fig. 3 Cross section of a cored cable

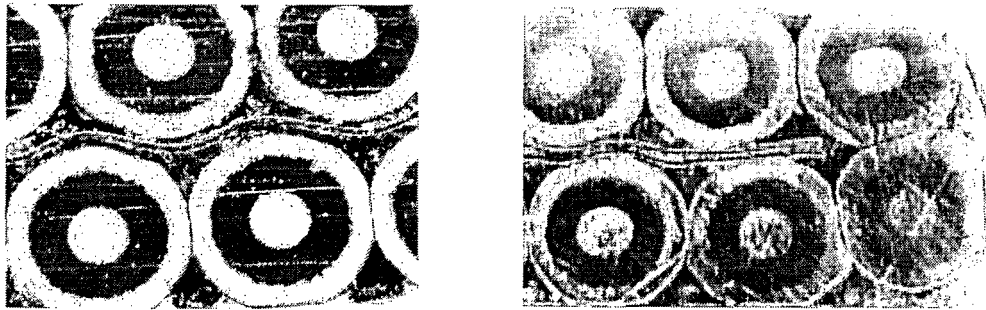


Fig. 4 Local region showing the stainless steel core foil in the middle and at the edge.

The initial cables were made at New England Wire Technology (NEWT) using a hollow mandrel, such that the foil was fed through the central hole of the hollow shaft of the cabling machine. Most of our experience is with stainless steel tapes. One of the problems encountered was the incidence of foil bunching in the cable, which was due to variation in the back-tension of the tape. Stainless steel tape needs to have very tight packages so that a high tension can be applied to prevent core-bunching. To eliminate post cleaning of the cable we used Wakefield 4BR vanishing lubricant that was dripped onto the mandrel which is the usual practice for cabling. Following an initial cabling run where cable lengths of $\sim 100\text{m}$ were made with SS and Ti-tapes, a longer cable of 600m using SS was fabricated with nominal RHIC dimensions. An examination of the core revealed another flaw; that of perforations of the foil at the strand cross-over region. Such perforations have been observed earlier in 12 μm SS-foils used in experimental LHC cables. The Ti-foil showed very significant perforations of the foil, whereas the SS-foil showed incidence of perforations only at the minor edge. Fig. 5 shows the nature of the perforation, which seems to be due to shear stress being applied to the foil after it has been compressed at the cross-over region.

From successive experimental cabling runs, we found that the incidence of perforation in SS-foil is greatly reduced by annealing the strands at 200C for several hours. The initial cables were made with fully cold-worked strands with RRR ~ 40 . Increasing the cable thickness by 15 μm also reduced the perforations by a factor of two. However, using the machine at NEWT, perforation free cables could not be fabricated using a single layer of SS-foil. Even using a lubricant like Mobil 1 along with 4BR was not very effective in solving this problem. Some of the other drawbacks of the hollow mandrel is making splice joints of the tape and excessive wear of the mandrel. This type of cabling needs additional work.

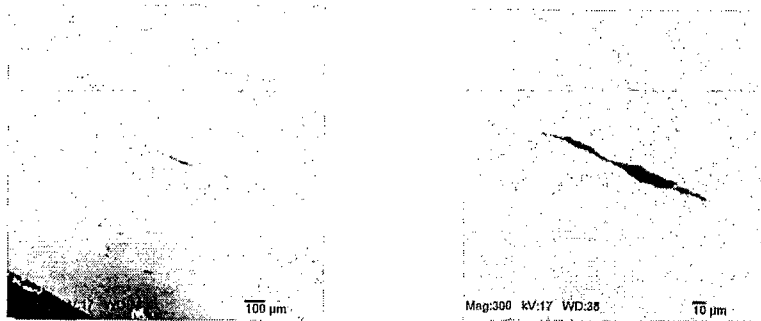


Fig. 5 SEM photograph of a perforation in the SS-foil

To fabricate perforation free cored cable, we resorted to using two layers of 25 μm thick SS-tape, and increasing the cable thickness to accommodate the extra layer. This was the type of cable that was finally used in the prototype magnet. We were also successful in making “good” cable with 50 μm Brass (95-5) tape with mid-thickness 10 μm over the nominal value of 1.166 mm. This foil by far is the easiest to use as a core. This might be due to the fact that Brass has an elastic modulus that matches the SC (superconducting)-wire and has good elongation property. Brass has an order of magnitude lower resistivity (3-6 $\mu\Omega\text{-cm}$) than SS which is typically $\sim 70 \mu\Omega\text{-cm}$. However the resistivity of the foil is not significant in determining R_C (see next section). An interesting candidate is Cu-30wt%Ni which has a resistivity of 38 $\mu\Omega\text{-cm}$ and a modulus that is slightly higher than the SC wire. An experimental cable has been fabricated by Lawrence Berkley Lab (LBL) which shows no foil perforation, and is being evaluated for inter-strand resistance.

Experimental cables were also fabricated at LBL where they use a slotted mandrel (cable has a solid shaft that is the most common situation) with the tape being fed close to the Turkshead. The “vanishing” lubricant 4BR was used. In this case perforation-free cored cable using a single layer of 25 μm thick SS-foil has been made. Periodic wrinkling of the foil is observed which will always be present due to the greater difference in the modulus of SS and the SC-wire. This cabling method is probably better than the hollow mandrel option as it would appear that single layer foils can be successfully used in the cable.

2.3 Interstrand Contact Resistances R_A and R_C of Cored Cables

A complete description of the electrical method to measure the interstrand contact resistances (ICR) is given in Ref. [12]. Most of what is described here can be found in Ref. [7] and Ref. [13].

Samples described here are from cable fabricated during two separate cabling runs (run GSI-003 and GSI-004) at New England Wire Technology (NEWT) and then insulated at BNL. The cable has standard RHIC insulation: two wraps of Kapton®, each 25 μm thick, with 50% overlap of each wrap, and a polyimide-based heat-set adhesive on the outside of the inner wrap and on both sides of the outer wrap, that bonds the different layers of the cable together after it has been cured. The samples are prepared as ten-stacks: 10 pieces of cable that are stacked on top of each other (with alternating keystone) and then cured. We use four spacer cables above and below the actual sample pieces; only the middle two cable pieces are tested. The 10 cable pieces are stacked into a fixture and cured. The curing cycle is the one used for the RHIC dipole magnets. It is shown in Fig. 6.

Much work has been done at CERN to optimize the coating of the strands in the superconducting dipoles for the Large Hadron Collider (LHC) [14-15]. As the LHC conductor is also coated with Sn-4%Ag solder, many of the mechanisms of oxide formation on the strands as described in the LHC references above are likely also at work in the cable described here. It is necessary to point out that, apart from the core, another fundamental difference between the LHC cable and the cable described here is the cable curing method: LHC curing is done with the curing pressure applied throughout. In the RHIC curing cycle, the pressure is completely released as the cable is heated from

135 °C to 225 °C (at which point a rather modest pressure of 7 MPa is applied to aid in the polyimide bonding). The pressure is also completely released as the cable is cooled from 225 °C to 135 °C. Thus oxidation is more likely to occur during this time for the RHIC procedure than for the LHC procedure as oxygen has easier access to the uncompressed wire surfaces than to compressed wire surfaces. Pre-annealing of the cable in air for durations of 2-8 hours was also evaluated.

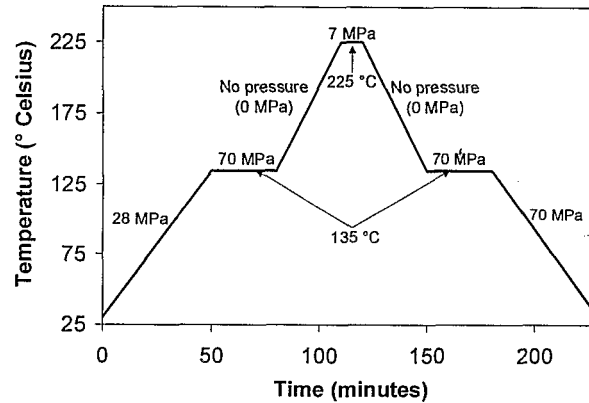


Fig. 6 RHIC Coil curing cycle

2.3.1 Results of the ICR Measurements

Each ten-stack contains two test samples; the results presented here are averages of the measured samples. In cases where the two samples in a ten-stack differed significantly, we prepared additional samples to clarify the results.

During the cabling run, GSI-003 six different cables were formed: Cables A and B both have a thinner Sn-4%Ag coating than the other cables and use annealed strands, cables A through D have a single 25 μm SS- foil, while cable E has two layers of the 25 μm SS-foil, and cable F has 1 layer of a 50 μm brass foil. For run GSI-004, segment A and B are made using 2 layers of SS-foil. Segment-B was used to fabricate the coils of the prototype magnet. The results are given in Table 2. The nominal mid-thickness for the RHIC cables is 1.166 ± 0.006 mm.

Table 2

R_A and R_C Results

	Sn-Ag Coating, μm	Cable Thickness, mm	Foil	R_A ($\mu\Omega$) After Cabling	R_A ($\mu\Omega$) 6 months later	R_C (m Ω)
GSI-003-A	0.66	1.138	25 μm SS	100	139	
GSI-003-B	0.66	1.180	25 μm SS	72	147	14
GSI-003-C	1.04	1.187	25 μm SS	28	80	
GSI-003-D	1.04	1.202	25 μm SS	18		12.5
GSI-003-E	1.04	1.173	2-25 μm SS	21.5	25	62.5
GSI-003-F	1.04	1.175	50 μm Brass	8.5	45	0.66
GSI-004-A	1.00	1.164	2-25 μm SS	55		
GSI-004-B	1.00	1.174	2-25 μm SS	74		

All the cored cables show an R_C significantly higher than R_A . In core-less cables, one typically finds $R_A \sim R_C$. The cables with the thinner Sn_{95%wt}Ag_{5%wt} coating (A and B) display a higher R_A which is likely caused by more oxidation due to the thinner coating. Furthermore, we also see that the thinner cables within a given coating thickness (A vs. B and C vs. D) show a higher R_A than the

thicker cables. We believe that the reason for this is increased compaction leads to better contact between the strands across the width of the cable. Also the data suggest that there is some aging effect on R_A . Experiments were also done which clearly show that R_A is significantly lower at the cable edge than it is along the flat area [7]. It is also interesting to note that for these same cables, R_A measured between 2.5-10 $\mu\Omega$ when the samples were cured without releasing the pressure at the intermediate steps. Pre-annealing the cable increased R_A significantly higher than the target value of 50-100 $\mu\Omega$

R_C for the cored cables is not significantly determined by the resistivity of the metal foil. It is mostly dominated by the surface contact between the strand and the foil. I speculate that the main effect comes from a mismatch of the mechanical properties of the foil and the strand. During cable formation at the Turkshead, the strand and the foil is stretched. After exiting the Turkshead the cable and the foil contracts with a relative difference. This shows up as periodic wrinkling of the SS-foil, which also implies that the strand-foil nesting is disturbed from the location at the point of cable formation. Brass seems to provide a lower surface contact resistance as its modulus matches that of the superconductor so that there is little differential shrinkage after the Turkshead.. Cables made with Cu-30wt%Ni are being evaluated. Loss measurements on 40cm long samples were also made at the University of Twente. The correlation with the resistance measurements was quite good. Details are in Ref. [6]

3. PROTOTYPE MAGNET PERFORMANCE

This section reports the successful initial test of a 1m fast-ramped superconducting model dipole built as part of the magnet R&D program for GSI. The magnet was designed to meet specifications for the SIS200 accelerator: 4 T central field, 1 T/sec ramp rate. Because the RHIC arc dipoles can operate at 4 T, GSI and BNL worked together on a model magnet program based on the RHIC design. Use of the RHIC cross-section enabled the work to take advantage of much of the RHIC design and tooling and some of the RHIC magnet components, thereby getting the effort off to a fast start. However, it has been necessary to make significant modifications to the magnet design, especially the superconductor (described in previous sections), to build a magnet that can ramp 20 times faster than RHIC and have much lower eddy current energy losses.

3.1 Magnet Construction

The cable used for coil fabrication was GSI-004-B, with the standard RHIC insulation. This insulation provides substantial impedance to the flow of helium between the interior of the cable and the reservoir just outside the coil. To allow more rapid heat exchange, a laser was used to cut away about 25% of the insulation on the thin edge of the insulated cable (Fig. 7). The holes in the insulation were precisely made so that the coils could be wound and cured without developing turn-to-turn shorts. Turn-to-turn standoff voltages of 1.1 kV were observed for both the straight section and end regions of a test coil that was cut in half and collared. This is less than the nominal test condition, > 2 kV, for RHIC coils but sufficient for the SIS200 application.



Fig. 7 Cable inner edge

Where feasible, magnet components were made from insulators rather than metals. In the GSI magnet (Fig. 2), the three wedges used in the coil to control field quality were G11 rather than Cu. The cable is ~ 25 μm thicker than the RHIC cable, resulting in a cured coil (32 turns) that is oversize by 0.9 mm. The G10 end pole spacers and Ultem® coil end saddles were modified to take account of the oversize cable. The shims placed between the coil and the pole were made of G11 and reduced in thickness to compensate for the oversized coil.

The coils were collared with Kawasaki high-Mn stainless steel collars. (The collars were designed for the LHC D2/D4 IR dipoles, also made using a variation of the RHIC arc dipole design.) As a handling aid, collars are assembled into 15 cm-long packs before being placed on the coils. G10 tubes were used to assemble these packs. It was possible to replace the brass keys used to lock the collars around the coils with G11 everywhere except for 2 cm at the non-lead end, where brass was used. At the lead end of the magnet, the collars have a larger inner diameter because of the radial space needed to bring the lead at the pole of the coil beyond the end of the coil. For the GSI magnet, the brass pieces used to fill this volume were halved in thickness and doubled in quantity, and the pieces of brass were insulated from one another.

The yoke laminations were 0.5 mm thick and punched from low coercivity 3.3% Si-steel ($H_c = 31 \text{ A/m}$). The laminations were coated with B-stage epoxy and glued into blocks 254 mm long. Five blocks make up a half yoke. Each half yoke is supported against axial motion by three stainless steel rods that run through holes in the yoke and restrain the yoke with stainless steel nuts insulated from the yoke by G10 washers. G10 tubes are placed around the stainless steel rods to insulate the rods from the yoke. The two yoke halves are aligned with respect to one another with G10 alignment keys at the yoke mid-plane. The yoke is held together by welding a stainless steel shell around it. There is a welding backup strip at the mid-plane but the strip is not welded to the yoke.

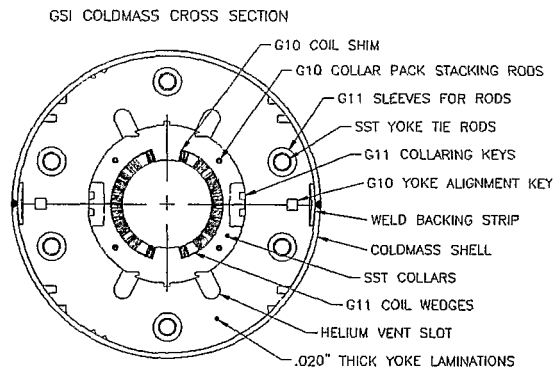


Fig 8. Cross section of the cold mass

In RHIC magnets, quenches at high ramp rate are likely to originate in the “ramp” section of the cable, at the end of the pole turn of the coil, where the cable is filled with solder to keep it rigid as it is moved by G10 fixtures to a larger radius so that it can be brought past the end of the coil and spliced to the cable from the other coil. The splice between the two coils halves is itself a possible source of quenching. However, the high value of R_c in the cored cable was judged to be sufficient to prevent such quenching in this magnet, so this region of magnet construction was the same as for RHIC dipoles. The magnet has no beam tube in it. Standard RHIC construction is used to restrain the axial motion of the coil.

3.2 QUENCH TEST RESULTS

The magnet was tested in pool boiling helium (4.5 K nominal). It was initially operated at the RHIC ramp rate, 0.053 T/s (Fig. 3). The sixth and last quench at this ramp rate was at 7.76 kA (4.38 T central field), approximately equal to the short-sample limit of the cable and ~ 10% above the 4 T

design. A different power supply was used for quenching at high ramp rate. It was found that both the magnet and this supply could ramp at 2 T/s, twice the design. Quench testing was carried out at this ramp rate. Further power supply improvements enabled the magnet to be ramped continuously to 4T and 4T/s without any quenches.

GSI001 QUENCH TESTS

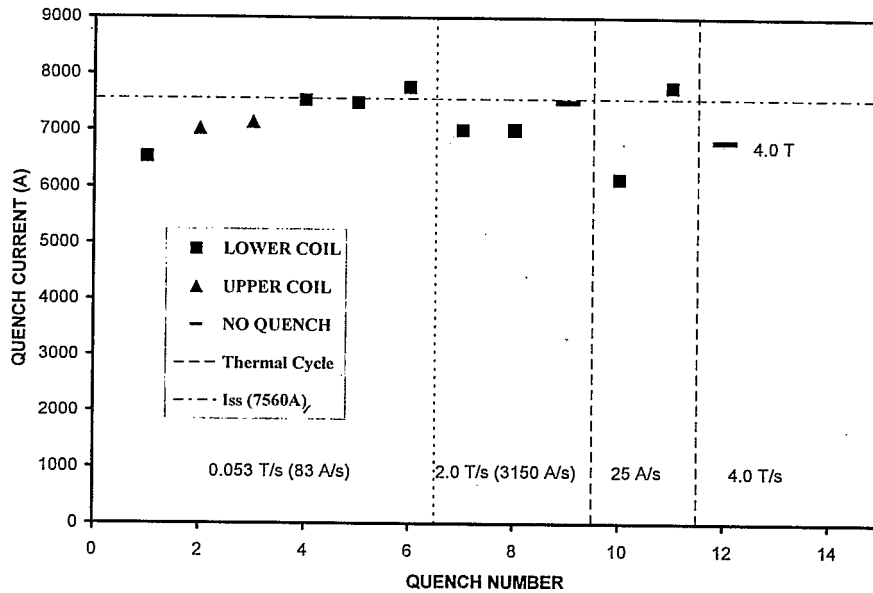


Fig. 9 Quench history, showing six quenches at 0.05 T/s, followed by two at 2 T/s, then stable operation at 7.5 kA. The horizontal line indicates the estimated short-sample limit of the magnet.

3.3 Loss Measurements

The energy loss was measured by recording the average voltage and current of the magnet over periods of 1/60 s. The cycle for a typical measurement is shown in Fig. 10

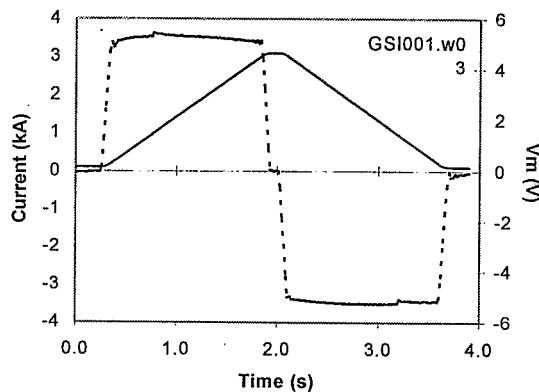


Fig. 10 Vm (dashed line) and I (solid line) for a typical energy loss measurement.

For each period, the energy was calculated as the VI product times the time between points. The magnet's voltage was measured by a precise voltmeter (HP3458A). The voltage taps on the magnet were placed on the superconducting leads, close to the coil (i.e., between the coil and the

splice that joins the magnet's leads and the power supply's leads). The current was measured by a voltmeter of the same model, which recorded the output of a DCCT (Holec).

A typical energy loss for this magnet is $\sim 0.2\%$ of the magnetic field energy, so considerable effort was invested in checking for and minimizing errors. The power supply control system was modified to minimize differences between the up ramp and the down ramp. The feedback circuit was adjusted to essentially eliminate overshoot. The control software generated smooth transitions between constant current and ramping. Each such transition accounted for typically 5% of the total ramp time. Dwell times at the minimum and maximum currents (typically 0.4 s and 0.2 s respectively) were minimized.

Two checks for offsets in the voltage were made with the power supply connected to the magnet but with the supply's reference input shorted. The first check was for DC offsets. There was no DC offset in the output voltage. Second, the effect of voltage errors was checked by programming the reference voltage to generate a fake, perfect current signal and measuring an apparent energy loss. For a 2 T/s ramp to 5 kA, an apparent loss of 1 J was measured, much smaller than the magnet's measured loss under these same conditions, ~ 80 J. The current offset is small, 0.2 A, and does not affect the measured energy loss.

Several other items should be mentioned. The measurement was not affected by the material used for the cryostat liner. We checked that the resistance of the splice between the two coil halves did not contribute measurably to the energy loss. Initially, measurements were made at constant dI/dt . At the highest ramp rates, we implemented an algorithm to correct for the $\sim 8\%$ drop in transfer function due to saturation at 4T so that the ramp would be at constant dB/dt . No significant difference was found between these measurements. The ramp rate quoted covers the entire time spent while ramping (including the smooth onset and roll-off of the ramp) but not the dwell times at high or low current. The AGS Booster Synchrotron, a possible source of perturbations of the 60 Hz AC signal, did not operate while these measurements were underway.

Details of the loss calculation in the magnet can be found in Ref. [9]. Fig. 11 shows the experimental measurements at select fields which are fitted to straight lines.

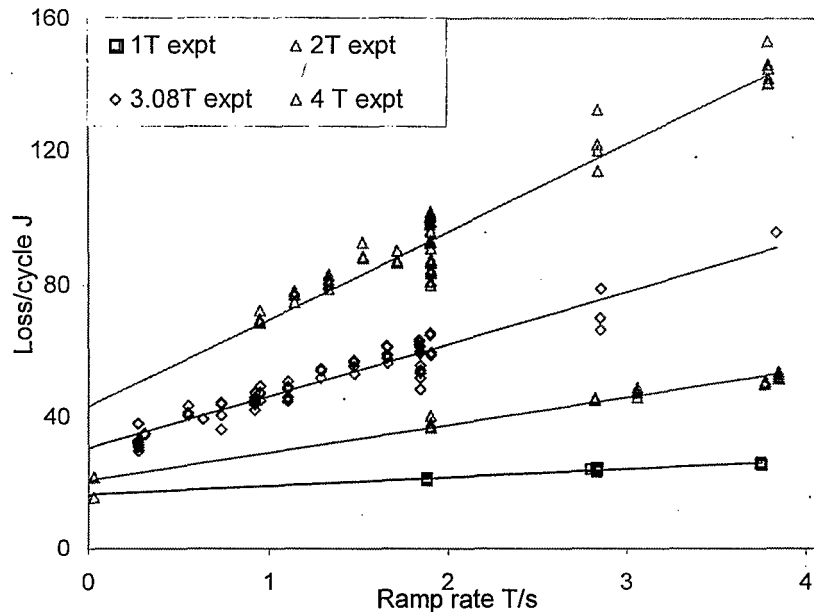


Fig 11. Experimental data of loss per cycle versus dB/dt for various values of maximum field

In order to compare the calculation with experimental data, the data points are fit to straight lines and the gradients (that due to eddy current loss) and intercepts (hysteresis loss) are compared with calculations. First we examine the rate dependent term which is assumed to be a sum of the strand loss and the cable loss. Fig. 12 shows the gradient plot. The eddy current losses are dominated by the inter-filament strand loss. The solid line is the inter-filament strand loss. The two dashed lines are for different assumptions about the cable coupling loss via R_A in transverse field. As noted in [6], this loss can be increased by up to a factor 3 if the R_A contact is predominantly at the edge of the cable and, as noted in [7], we have seen clear indication that R_A is lower at the edge than in the centre. The calculation uses the following measured quantities: $R_C=60$ m Ω , $R_A=64$ $\mu\Omega$, and matrix resistivity $\rho_{et}=1.1 \times 10^{-10}$ $\Omega\cdot\text{m}$. Also shown is a quadratic fit to the data (dot-dash line). From Fig. 12, it would appear that the edge concentration gets stronger at high fields, perhaps an effect of the increasing forces.

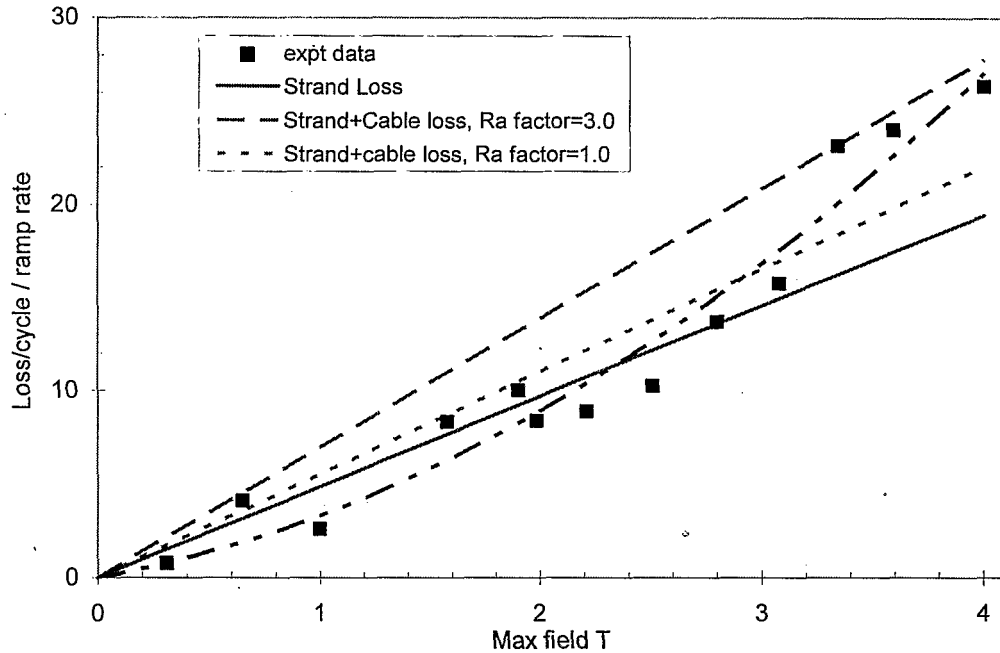


Fig 12 Experimental and calculated gradient of (loss per cycle vs. ramp rate) vs. maximum field.

Secondly the intercept of the plots in Fig. 11 at zero ramp-rate, which is the hysteresis loss per cycle, is plotted. Theoretically, this loss comprises three terms: the superconductor hysteresis loss, the enhancement caused by transport current and the iron loss. Fig 13 shows each of the calculated terms. It may be seen that the transport current correction has not made much difference. The iron hysteresis makes an increasing contribution at high fields, but does not fully explain the upward curvature of the experimental data. Nevertheless, the general level of agreement is reasonably good.

4. CONCLUSIONS

Even in the fastest sweeps of 4T/s to 4T, the 4T-model dipole has shown no effect of ramp rate on quench current. AC losses show the expected behaviour of a hysteresis component plus a component comprising coupling and eddy currents, which increases linearly with ramp rate. Using a set of parameters derived from measurements on short samples of wire and cable, we have calculated hysteresis and rate dependent components of loss which are in very reasonable agreement with the measured losses. The rate dependent losses seem to confirm that our conductor has an adjacent

resistance R_A which is lower at the edge of the cable than in the centre and that, perhaps, this effect gets stronger at high fields, i.e. at high stresses. Hysteresis loss is generally as predicted, but the experimental plots show a somewhat stronger upward curvature at high fields; we have no explanation for this.

Overall, the lack of an effect of ramp rate on quench current and the rather low and predictable ac losses show that this method of coil construction is very suitable for fast ramping accelerator magnets.

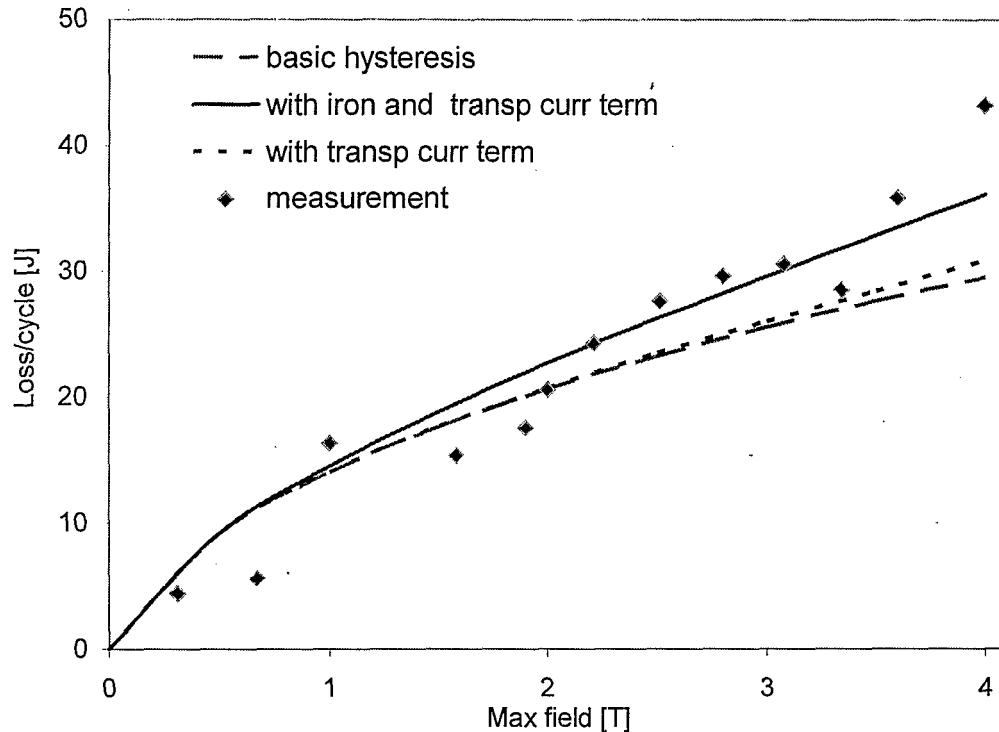


Fig. 13 Calculated and experimental data of hysteresis loss per cycle (intercept of loss vs. dB/dt plots).

ACKNOWLEDGEMENTS

I would like to acknowledge the work of all the collaborators on the GSI prototype magnet development. They are the following: from BNL, M. Anerella, G. Ganetis, P. Joshi, A. Marone, J. Muratore, J. Schmalzle, R. Soika, R. Thomas, P. Wanderer, from GSI, C. Muehle, J. Kaugerts, G. Moritz, and Consultants to GSI, M. N. Wilson, W.V. Hassenzahl.

This work was supported in part by the U.S. Department of Energy under Contract No. DE-AC02-98CH10886

REFERENCES

- [1] G. Moritz et al, "Towards Fast-Pulsed Superconducting Synchrotron Magnets," Proc. 2001 Particle Accelerator Conf. (2001) 211.
- [2] A.D. Kovalenko et al, "Superferric Model Dipole Magnet with the Iron Yoke at 80K for the GSI Future Fast Cycling Synchrotron", IEEE Trans Appl Superconductivity, Vol 13 (2003) 1335.
- [3] M. Anerella et al, "The RHIC Magnet System," Nucl. Inst. Meth. A, Vol 499,(2003) 280.

- [4] D. Wake, D. Gross, R. Yamada and B Blatchley, IEEE Trans MAG-15, No 1,(1979) 141.
- [5] M.N. Wilson et al, "Design Studies on Superconducting $\cos\theta$ Magnets for a Fast Pulsed Synchrotron", Proc MT-17, IEEE Trans. Appl. Superconductivity Vol 12, (2002) 313.
- [6] R. Soika et al, "Inter-strand Resistance Measurements in Cored Rutherford Cables", IEEE Trans Appl Superconductivity, Vol 13 (2003) 2380.
- [7] M.N. Wilson, A.K. Ghosh, B. ten Haken, W.V. Hassenzahl, J. Kaugerts, G. Moritz, C. Muehle, A. den Ouden, R. Soika, P. Wanderer, W. A. J. Wessel, "Cored Rutherford Cables for the GSI Fast Ramping Synchrotron", IEEE Trans Appl Superconductivity, Vol 13, (2003) 704.
- [8] P.Wanderer et al, "Initial test of a fast-ramped superconducting model dipole for GSI's proposed SIS200 accelerator", Proc. 2003 Particle Accelerator Conference, Portland OR USA, May 12- 16, 2003,
- [9] M. Wilson et al, "Measured and calculated losses in a model dipole for GSI's Heavy Ion synchrotron", MT-18 Morioka, Japan, Oct 20-24, 2003.
- [10] S. Le Naour, "Test Report on Magnetization measurements made on RHIC wires with CERN test station", CERN Tech. Note 2003-03, (2003)
- [11] A. K. Ghosh, W. B. Sampson, E. Gregory, S. Kreilick, and J. Wong, "The effect of magnetic impurities and barriers on the magnetization and critical current of fine filament NbTi composites", IEEE. Trans. on Magnetics, vol. 24, (1988) 1145.
- [12] A. P. Verweij, Electrodynamics of Superconducting Cables in Accelerator Magnets, Ph.D. Thesis, University of Twente, Enschede, The Netherlands, (1995).
- [13] R. Soika and A.K. Ghosh, "Interstrand resistances in cored Rutherford-type superconducting cables", submitted to Cryogenics (2004).
- [14] D. Richter, J. D. Adam, J.-M. Depond, D. Leroy, and L. R. Oberli, "DC Measurement of Electrical Contacts between Strands in Superconducting Cables for the LHC Main Magnets", IEEE Trans. Appl. Superconductivity, vol. 7, (1997) 786.
- [15] D. Richter, J. D. Adam, D. Leroy, and L. R. Oberli, "Strand Coating for the Superconducting Cables of the LHC Main Magnets", IEEE Trans. Appl. Superconductivity., vol. 9 (1997) 735.